Modulated photocurrents in a sandwich-cell structure

2000 J. Phys.: Condens. Matter 12 5209

(http://iopscience.iop.org/0953-8984/12/24/312)

J. Phys.: Condens. Matter **12** (2000) 5209–5223. Printed in the UK PII: S0953-8984(00)10528-4

Modulated photocurrents in a sandwich-cell structure

P Grygiel and W Tomaszewicz

Department of Technical Physics and Applied Mathematics, Technical University of Gdańsk, Narutowicza 11/12, 80-952 Gdańsk, Poland

E-mail: pgrygiel@sunrise.pg.gda.pl and wtomasze@sunrise.pg.gda.pl

Received 23 December 1999, in final form 10 April 2000

Abstract. Approximate formulae describing modulated photocurrents in a sandwich configuration of sample electrodes are derived. The carrier transport is described in terms of the multiple-trapping model. The formulae refer to arbitrary spatial distribution of generated carriers. The case of exponential light absorption in the sample is considered in detail. It is shown that for limiting low and high modulation frequencies, both the amplitude and the phase shift of the photocurrent are almost independent of the light absorption coefficient. In the intermediate-frequency range, for the case of surface carrier generation, the phase shift of the photocurrent usually shows oscillations. This makes it possible to obtain the energetic density of states from a simple formula. Examples of calculated frequency dependencies of the photocurrent phase shift and amplitude are given for exponential and Gaussian trap distributions as well as for a single trap level.

1. Introduction

The density of states (DOS) in the forbidden gap of a disordered solid has been studied extensively for a number of years using various experimental methods. Among others, techniques using a sinusoidally modulated photocurrent (MPC) have been developed. They are based on light excitation of charge carriers in the sample and frequency-dependent measurements of the response signal. The MPC method combined with modern measuring techniques provides an important alternative to time-domain experiments, e.g. using the time-of-flight (TOF) method, and affords possibilities for determining the DOS distribution in an extended energy interval.

The MPC technique has been used in two types of experiment that differ in sample electrode configuration. Most papers published so far concern coplanar electrode geometry. The theoretical description of the method has been developed by Oheda [1] who also gave a recursion procedure using the MPC phase shift for calculating the DOS distribution and applied it to CdS crystals. Later on, alternative approaches for analysis of the experimental data were suggested by Brüggemann *et al* [2] as well as Hattori *et al* [3]. The authors used simple expressions containing both the phase shift and the modulus of the MPC for determining the DOS energy profile and applied them to *a*-As_2Se_3 and *a*-Si:H. That the technique can be used for investigating the localized-states distribution has been proved by means of numerous experiments carried out on amorphous solids [4–8]. A comprehensive theoretical analysis of the method, including the contribution of both electron and hole components to the MPC as well as the influence of correlated defects in the energy gap, has been carried out by Longeaud and Kleider [9, 10]. Hence, at present, one may regard the theory of the MPC in coplanar electrode geometry as well mastered and complete.

0953-8984/00/245209+15$30.00

The MPC method has also been employed in experiments carried out on the sandwich (TOF) electrode configuration. This extension has been proposed by Schumm and Bauer [11], who adopted the modified analytical technique developed by Oheda and applied it to *a*-Si:H. They have concluded that, in addition to the energetic profile, the spatial distribution of localized states can also be determined. More recently, the sensitivity of this technique was examined by Brüggemann *et al* [12] by means of numerical simulation for different light absorption depths. Measurements of the MPC in *a*-Si:H in the sandwich sample configuration were also carried out by Amato *et al* [13] and Cohen and Zhong [14]. It is worth noting that in the former paper a distinct dependence of both the phase shift and the amplitude of the MPC on the exciting light wavelength was established. More detailed theoretical description of the experiment concerning the surface carrier generation has been published by Tomaszewicz [15] and Hattori *et al* [7]. As noted in these papers, in both the low- and the high-frequency domain the formulae for MPC are considerably simplified and enable us to calculate the DOS energetic profile.

The present work is a continuation of investigations reported in the latter two papers. The formulae describing MPCs have been derived for the case of an arbitrary spatial distribution of carriers generated in the specimen. It has been demonstrated that for a large light absorption coefficient the phase shift of the MPC usually shows oscillations in a certain range of modulation frequencies. This behaviour also makes it possible to determine the energetic profile of the DOS. Moreover, a detailed analysis of the frequency dependence of the photocurrent has been carried out for several model trap distributions.

2. Formulation of the problem

The present paper concerns the usual experimental set-up for investigations of MPCs in a sandwich-cell structure. The sample has the form of a thin layer, sandwiched between two plane-parallel electrodes with a constant voltage applied to them. The carrier photogeneration or photoinjection is accomplished by illuminating one semi-transparent electrode with a modulated light beam. The carrier drift in the electric field takes place in the direction perpendicular to the electrodes.

2.1. Simplifying assumptions

The carrier transport in the sample is described in terms of the usual multiple-trapping (MT) model. In order to make the problem tractable analytically, some simplifying assumptions have been introduced.

(i) The measured MPC is due to the transport of carriers of only one sign, e.g. electrons. This assumption seems to be justified if, for example, the carriers are photogenerated in a surface layer of the sample that is relatively thin, compared to the sample thickness. Then, the contribution to the MPC of the hole transport in the carrier-generation region should be negligible.

(ii) The applied field is so high that the carrier recombination in the illuminated sample layer as well as the carrier diffusion can be ignored. The rough criterion for omitting the diffusion effect has been given in [15].

(iii) The density of carriers thermally generated in the sample is very low, compared with the photocarrier density (the case of an insulating solid). This means that the Maxwell relaxation time, corresponding to dark conductivity of a solid, is much longer than the characteristic times of the phenomena considered.

(iv) The electrodes do not inject carriers into the sample, and quickly neutralize the carriers of opposite sign arriving at them.
(v) The possible energy dependence of the carrier capture coefficient and frequency factor is ignored.

The above assumptions are essentially the same as in the earlier papers on the subject [7,12,15].

2.2. Transport equations

The above-mentioned model of carrier transport corresponds to the following set of equations:

$$\frac{\partial n(x,t)}{\partial t} = g(x,t) - \mu_0 \frac{\partial}{\partial x}\left[n(x,t)E(x,t)\right] - C_t \left\{\int_0^\infty \left[N_t(\varepsilon) - n_t'(x,t,\varepsilon)\right] \mathrm{d}\varepsilon\right\} n(x,t) + \int_0^\infty \frac{n_t'(x,t,\varepsilon)}{\tau_r(\varepsilon)} \mathrm{d}\varepsilon \tag{1}$$

$$\frac{\partial n_t'(x,t,\varepsilon)}{\partial t} = C_t \left[N_t(\varepsilon) - n_t'(x,t,\varepsilon)\right] n(x,t) - \frac{n_t'(x,t,\varepsilon)}{\tau_r(\varepsilon)} \tag{2}$$

$$\frac{\partial E(x,t)}{\partial x} = \frac{e}{\kappa\kappa_0}\left[n(x,t) + n_t(x,t)\right] \tag{3}$$

where

$$n_t(x,t) = \int_0^\infty n_t'(x,t,\varepsilon)\, \mathrm{d}\varepsilon. \tag{4}$$

Here, x is the distance from the front electrode of the sample, t and ε denote, respectively, the time and energy variables (energy ε is measured from the edge of the conduction band), $n(x,t)$ and $n_t(x,t)$ are the free- and trapped-carrier densities, $n_t'(x,t,\varepsilon)$ is the density of trapped carriers per unit of energy, $g(x,t)$ is the carrier generation rate and $E(x,t)$ denotes the electric field strength. The meaning of the remaining notation is as follows: μ_0 is the microscopic carrier mobility, e the elementary charge, κ the dielectric constant, κ_0 the permittivity of free space, C_t the carrier capture coefficient, $N_t(\varepsilon)$ the trap density per energy unit and $\tau_r(\varepsilon) = \nu_0^{-1}\exp(\varepsilon/kT)$ the mean carrier dwell time in the trap (ν_0 is the frequency factor, k the Boltzmann constant and T the sample temperature).

Equation (1) is the continuity equation. It states that the time variation of the free-carrier density is due to the carrier generation, drift, capture and release from the traps (the sequential terms on the RHS). Equation (2) describes the change of trapped-carrier density at a given energy level ε, caused by the carrier capture and emission processes (the first and the second term on the RHS). Equation (3) is Poisson's equation, determining the relationship between the electric field and the total carrier density. The hole density is here omitted, since it is assumed to be negligible outside the illuminated sample layer. Integrating equation (2) with respect to energy and adding it to equation (1) gives another form of the continuity equation:

$$\mu_0 \frac{\partial}{\partial x}\left[n(x,t)E(x,t)\right] + \frac{\partial}{\partial t}\left[n(x,t) + n_t(x,t)\right] = g(x,t). \tag{5}$$

Since there is no carrier injection from the front electrode and the carrier diffusion is neglected, the boundary condition for the above equations can be written as follows:

$$n(0,t) = 0. \tag{6}$$

This implies that the total current at the illuminated electrode is the sum of the hole conduction current and the displacement current. The electric field fulfils the condition

$$\int_0^d E(x,t)\, \mathrm{d}x = V \tag{7}$$

where V is the constant voltage applied to the sample.

The current intensity, $I(t)$, induced in the measuring circuit equals the spatial average of the conduction current in the specimen (see, e.g., [16]):

$$I(t) = \frac{e\mu_0 S}{d} \int_0^d n(x,t)E(x,t)\,\mathrm{d}x \tag{8}$$

where S is the sample area and d is the sample thickness. Here, the hole component of the conduction current is neglected.

2.3. Linearized transport equations

In the MPC experiment, generation of carriers is due to illumination varying sinusoidally with time. Making the assumption that the free-carrier generation rate is proportional to the light intensity, one can write

$$g(x,t) = g_0(x) + \Delta g(x)\exp(\mathrm{i}\omega t) \tag{9}$$

where ω is the angular frequency of the light modulation. We will consider only the linear response of the sample to the excitation which is expected to occur for shallow light modulation, $\Delta g(x) \ll g_0(x)$. The solutions of equations (2)–(5) should then also consist of the dc and ac terms, the latter being proportional to $\exp(\mathrm{i}\omega t)$. In what follows, these terms will be indicated respectively by the subscript '0' and the symbol 'Δ', e.g.

$$n(x,t) = n_0(x) + \Delta n(x)\exp(\mathrm{i}\omega t). \tag{10}$$

Here, $\Delta n(x)$ is the complex function that determines both the phase shift and the amplitude of the oscillating carrier density. According to the common convention, only real parts of the expressions are of physical significance. In order to simplify the notation, in sections 2.3–3.4 and in the appendices we shall not indicate the dependence of the functions on ω.

Inserting these expressions into equations (5), (2) and (3) and retaining only the first-order ac terms, we obtain

$$\mu_0 \frac{\mathrm{d}}{\mathrm{d}x}\left[E_0(x)\,\Delta n(x) + n_0(x)\,\Delta E(x)\right] + \mathrm{i}\omega\left[\Delta n(x) + \Delta n_t(x)\right] = \Delta g(x) \tag{11}$$

$$\Delta n_t'(x,\varepsilon) = \frac{C_t\left[N_t(\varepsilon) - n_{t_0}'(x,\varepsilon)\right]}{\mathrm{i}\omega + C_t n_0(x) + 1/\tau_r(\varepsilon)}\,\Delta n(x) \tag{12}$$

and

$$\frac{\mathrm{d}\,\Delta E(x)}{\mathrm{d}x} = \frac{e}{\kappa\kappa_0}\left[\Delta n(x) + \Delta n_t(x)\right]. \tag{13}$$

From conditions (6) and (7) one gets

$$n_0(0) = 0 \tag{14}$$

$$\Delta n(0) = 0 \tag{15}$$

and

$$\int_0^d E_0(x)\,\mathrm{d}x = V \tag{16}$$

$$\int_0^d \Delta E(x,t)\,\mathrm{d}x = 0. \tag{17}$$

Integrating equation (12) with respect to the energy, we get the equation

$$\Delta n_t(x) = \tilde{\Phi}(x)\,\Delta n(x) \tag{18}$$

where the function

$$\tilde{\Phi}(x) = C_t \int_0^\infty \frac{\left[N_t(\varepsilon) - n'_{t_0}(x,\varepsilon)\right] \mathrm{d}\varepsilon}{\mathrm{i}\omega + C_t n_0(x) + 1/\tau_r(\varepsilon)}. \tag{19}$$

$\tilde{\Phi}(x)$ is the Fourier transform of the carrier release-time distribution function

$$\Phi(x) = C_t \int_0^\infty \left[N_t(\varepsilon) - n'_{t0}(x,\varepsilon)\right] \exp\{-[C_t n_0(x) + 1/\tau_r(\varepsilon)]t\} \,\mathrm{d}\varepsilon \tag{20}$$

(see [17]); that is,

$$\tilde{\Phi}(x) = \int_0^\infty \exp(-\mathrm{i}\omega t)\Phi(x) \,\mathrm{d}t. \tag{21}$$

As shown in appendix A, the function $\tilde{\Phi}(x)$ can be written in the simplified form

$$\tilde{\Phi}(x) \simeq C_t \int_0^{\varepsilon_f(x)} \frac{N_t(\varepsilon) \,\mathrm{d}\varepsilon}{\mathrm{i}\omega + 1/\tau_r(\varepsilon)} \tag{22}$$

where

$$\varepsilon_f(x) = kT \ln[\nu_0/C_t n_0(x)] \tag{23}$$

is the quasi-Fermi level. According to equation (8), the expression describing the ac component of the photocurrent has the form

$$\Delta I = \frac{e\mu_0 S}{d} \int_0^d [E_0(x)\,\Delta n(x) + n_0(x)\,\Delta E(x)] \,\mathrm{d}x. \tag{24}$$

In the next section, the above set of equations is approximately solved and the formulae for the MPC in the measuring circuit are given.

3. Analytical results

3.1. General solution

Further on, we shall simplify the set of equations considered, neglecting the term $n_0(x)\,\Delta E(x)$ in equations (11) and (24). The more detailed calculations, given in appendix B, show that the approximation is valid in the frequency range $\omega \gg 1/\tau_M$ ($\tau_M = \kappa\kappa_0/e\mu_0 n_0$ is the Maxwell relaxation time with n_0 the average free-carrier density). Then, inserting (18) into (11) and integrating the equation obtained, using the boundary condition (15), we obtain the formula

$$\Delta n(x) = \frac{1}{\mu_0 E_0(x)} \int_0^x \Delta g(x') \exp\left[-\frac{\mathrm{i}\omega}{\mu_0} \int_{x'}^x \frac{1 + \tilde{\Phi}(x'')}{E_0(x'')} \,\mathrm{d}x''\right] \mathrm{d}x' \tag{25}$$

and, from equation (24), the expression for the MPC:

$$\Delta I = \frac{eS}{d} \int_0^d \int_0^x \Delta g(x') \exp\left[-\frac{\mathrm{i}\omega}{\mu_0} \int_{x'}^x \frac{1 + \tilde{\Phi}(x'')}{E_0(x'')} \,\mathrm{d}x''\right] \mathrm{d}x' \,\mathrm{d}x. \tag{26}$$

In order to calculate the MPC for a given trap distribution, the form of the functions $n_0(x)$, $n'_{t0}(x,\varepsilon)$ and $E_0(x)$ must be known. For this purpose one has to solve the corresponding set of equations, which results from equations (2)–(5). The problem is similar to the case of emission-limited or space-charge-limited currents (see, e.g., [18]) and in general can be treated only numerically. Moreover, equation (26) is too complicated to be useful in the analysis of experimental data. Therefore, in the following formulae we shall ignore the spatial dependence of $E_0(x)$ and $\tilde{\Phi}(x)$, and assume that $E_0(x) \simeq V/d$. The approximation should be valid for

relatively low generation rates of the carriers, when the space charge in the sample does not significantly disturb the external field. After slight rearrangements of equations (25) and (26), one then gets

$$\Delta n(x) = \frac{d}{\mu_0 V}\int_0^x \Delta g(x-x')\exp\left[-\frac{\mathrm{i}\omega d}{\mu_0 V}(1+\tilde{\Phi})x'\right]\,\mathrm{d}x' \tag{27}$$

$$\Delta I = \frac{eS}{\mathrm{i}\omega\tau_0(1+\tilde{\Phi})}\int_0^d \Delta g(d-x)\left\{1-\exp\left[-\frac{\mathrm{i}\omega d}{\mu_0 V}(1+\tilde{\Phi})x\right]\right\}\,\mathrm{d}x \tag{28}$$

with $\tau_0 = d^2/\mu_0 V$—the free-carrier time of flight.

Next, we shall write the MPC as

$$\Delta I = \Delta I_m \exp(-\mathrm{i}\varphi_I) \tag{29}$$

where ΔI_m and φ_I denote the MPC amplitude and phase shift, measured in the experiment. These quantities can be calculated by comparison of equations (28) and (29). We shall also adopt the following notation [15]:

$$\varphi = \omega\tau_0[1+\mathrm{Re}\,\tilde{\Phi}] = \omega\tau_0\left[1+C_t\int_0^{\varepsilon_f}\frac{N_t(\varepsilon)\tau_r(\varepsilon)}{1+\omega^2\tau_r^2(\varepsilon)}\,\mathrm{d}\varepsilon\right] \tag{30}$$

$$\gamma = -\omega\tau_0\,\mathrm{Im}\,\tilde{\Phi} = \omega^2\tau_0 C_t\int_0^{\varepsilon_f}\frac{N_t(\varepsilon)\tau_r^2(\varepsilon)}{1+\omega^2\tau_r^2(\varepsilon)}\,\mathrm{d}\varepsilon. \tag{31}$$

In the case of surface carrier generation, $\Delta g(x) \propto \delta(x)$ (with $\delta(\cdots)$ the Dirac delta function); φ is the phase shift and γ is the 'damping coefficient' of the free-carrier-density wave, related by the formula

$$\Delta n(d) = \Delta n(0+)\exp(-\mathrm{i}\varphi - \gamma) \tag{32}$$

which results from (27). As far as an amorphous solid is concerned, the term $\omega\tau_0$ in equation (30) is negligibly small compared to the second one and can be omitted. Moreover, for a wide distribution of localized states, varying slowly in the kT-energy range, equations (30) and (31) can be approximated as follows [7, 15]:

$$\varphi \simeq \frac{\pi}{2}\tau_0 kT C_t N_t(\varepsilon_0) \tag{33}$$

$$\gamma \simeq \tau_0 C_t\int_{\varepsilon_0}^{\varepsilon_f} N_t(\varepsilon)\,\mathrm{d}\varepsilon \tag{34}$$

for $0 < \varepsilon_0 < \varepsilon_f$. Here, ε_0 denotes the demarcation level at which the release time of a trapped carrier $\tau_r(\varepsilon_0) = 1/\omega$ [1]; that is,

$$\varepsilon_0 = kT\ln(\nu_0/\omega). \tag{35}$$

In the following subsections, the approximate formulae for the MPC are given for several ranges of modulation frequency.

3.2. High-frequency domain

In the high-frequency range yielding strong damping of the carrier-density wave, $\gamma > 1$, the exponential term in the integrand in equation (28), may be omitted. Therefore, the expression for ΔI takes the simple form

$$\Delta I \simeq \frac{\Delta I_0}{\gamma + \mathrm{i}\varphi} \tag{36}$$

where ΔI_0 is the normalization factor for the current intensity:

$$\Delta I_0 = eS \int_0^d \Delta g(x)\, \mathrm{d}x. \tag{37}$$

The amplitude and phase shift of the photocurrent are described by the formulae

$$\Delta I_m \simeq \Delta I_0 \left[\varphi^2 + \gamma^2\right]^{-1/2} \tag{38}$$

$$\tan \varphi_I \simeq \varphi/\gamma. \tag{39}$$

We note that equation (39), with φ and γ given by (33) and (34), has a form analogous to the expression obtained by Oheda [1] in which the carrier-recombination term is neglected. Thus the shape of the function $N_t(\varepsilon)$ can be determined using the method developed by Brüggemann *et al* [2] or Hattori *et al* [3]. It should be stressed that in this frequency range the carrier diffusion may, however, play a significant role.

3.3. Low-frequency domain

For low modulation frequencies, when $\gamma, \varphi \ll 1$ (weak damping of the carrier-density wave) and $\varphi \simeq \gamma$, the exponential function in the integrand of equation (28) can be expanded into a power series, which gives

$$\Delta I \simeq c_1\, \Delta I_0 (1 - \mathrm{i} c_2 \varphi) \tag{40}$$

with coefficients c_1 and c_2 defined by

$$c_1 = \int_0^d \left(1 - \frac{x}{d}\right) \Delta g(x)\, \mathrm{d}x \Big/ \int_0^d \Delta g(x)\, \mathrm{d}x \tag{41}$$

$$c_2 = \int_0^d \left(1 - \frac{x}{d}\right)^2 \Delta g(x)\, \mathrm{d}x \Big/ 2 \int_0^d \left(1 - \frac{x}{d}\right) \Delta g(x)\, \mathrm{d}x. \tag{42}$$

In particular, in the case of surface carrier generation, $c_1 = 1$ and $c_2 = 1/2$. The expressions for the amplitude ΔI_m and phase shift φ_I of the photocurrent take the forms

$$\Delta I_m \simeq c_1\, \Delta I_0 \tag{43}$$

and

$$\varphi_I \simeq c_2 \varphi. \tag{44}$$

Therefore, the shape of the function $N_t(\varepsilon)$ can be directly determined using equations (44) and (33). This is an extension of the formulae obtained in [7, 11, 15].

3.4. Intermediate-frequency domain

In the intermediate-frequency range, each of the functions φ_I and ΔI_m has a complicated form and depends, apart from the trap distribution, on the light absorption depth. For this reason, only some features of MPCs can be then established.

We note first that the results obtained in two last subsections apply, respectively, for $\gamma > 1$ and $\gamma \ll 1$. Therefore, the limiting frequency ω_e between the low- and high-frequency regimes is determined implicitly by the condition $\gamma \simeq 1$. In the case of a trap distribution slowly varying with energy, from equations (34) and (35) we get the formula

$$\tau_0 C_t \int_{\varepsilon_{0e}}^{\varepsilon_f} N_t(\varepsilon)\, \mathrm{d}\varepsilon \simeq 1 \tag{45}$$

where

$$\varepsilon_{0e} = kT \ln(\nu_0/\omega_e). \tag{46}$$

For the surface carrier-generation case the analogous formulae were obtained first in [7]. The formulae make it possible to determine the form of the integrated DOS function in the interval $\varepsilon_{0e} \leqslant \varepsilon \leqslant \varepsilon_f$ from the measured dependence of ω_e on the voltage V, applied to the sample, and/or on the sample thickness d. However, the frequency ω_e corresponds to the crossover point of the extrapolated curves, representing the function φ_I or ΔI_m for $\omega \ll \omega_e$ and $\omega > \omega_e$, and cannot be determined exactly.

Another feature of MPCs in the intermediate range of frequency is the oscillatory behaviour of the phase shift φ_I and the corresponding anomalies of the amplitude ΔI_m. We shall demonstrate this for the case of surface carrier generation, $\Delta g(x) \propto \delta(x)$. Then, the final expressions for the phase shift and amplitude of MPC, obtained from equations (28) and (29), are

$$\Delta I_m = \Delta I_0 \left\{ \frac{\left[1 - \exp(-\gamma)\cos\varphi\right]^2 + \left[\exp(-\gamma)\sin\varphi\right]^2}{\varphi^2 + \gamma^2} \right\}^{1/2} \tag{47}$$

and

$$\tan\varphi_I = \frac{\varphi\left[1 - \exp(-\gamma)\cos\varphi\right] - \gamma\exp(-\gamma)\sin\varphi}{\gamma\left[1 - \exp(-\gamma)\cos\varphi\right] + \varphi\exp(-\gamma)\sin\varphi}. \tag{48}$$

For weakly dispersive carrier transport, when the ratio $\varphi/\gamma \gtrsim 1$, the maxima of φ_I occur for the values of φ_n given approximately by $\sin\varphi_n \simeq -1$; that is,

$$\varphi_n \simeq \frac{(4n-1)\pi}{2} \qquad n = 1, 2, 3, \ldots. \tag{49}$$

Since γ increases with frequency ω (cf. equations (34) and (35)), for increasing frequency the oscillations are more and more strongly damped. At first sight, one can also expect the existence of local maxima of the MPC amplitude ΔI_m at the same values of φ_n. For dispersive carrier transport, however, only some anomalies in the course of ΔI_m can be recognized (cf. the next section). Making use of equation (33), one gets the formula

$$N_t(\varepsilon_{0n}) \simeq \frac{4n-1}{C_t kT\tau_0} \qquad n = 1, 2, 3, \ldots \tag{50}$$

where

$$\varepsilon_{0n} = kT \ln(\nu_0/\omega_n) \tag{51}$$

and the ω_n denote the positions of φ_I-maxima. The above expressions enable us to calculate the DOS profile from the dependence of ω_n on the applied voltage V and/or the sample thickness d, measured in the experiment. The above-proposed treatment is analogous to the method of the DOS calculation in the TOF measurements from the dependence of the effective carrier transit time on V and/or d [19].

The oscillations of φ_I should also occur for the case of non-dispersive carrier transport, e.g. due to a single trapping level of depth ε_m, provided that the condition $\varphi/\gamma \gtrsim 1$ is fulfilled. Since for a discrete trap level the ratio $\varphi/\gamma = 1/\omega\tau_r(\varepsilon_m)$, as follows from (30) and (31), the oscillations can appear only in the frequency interval $\omega \lesssim 1/\tau_r(\varepsilon_m)$. The formulae (50) and (51) are then not valid, since they refer to a continuous trap density.

In the present calculations the effect of carrier diffusion is disregarded. One can expect the carrier diffusion to cause some 'smearing out' of the φ_I-peaks, but those corresponding to the lowest values of n can still be distinguished.

4. MPCs for model trap distributions

In order to investigate the detailed behaviour of the MPCs, we have performed calculations of the functions $\varphi_I(\omega)$ and $\Delta I_m(\omega)$ for three model trap distributions: the exponential one

$$N_t(\varepsilon) = \frac{N_{tot}}{kT_c} \exp\left(-\frac{\varepsilon}{kT_c}\right) \tag{52}$$

and the ε_m-peaked Gaussian distribution

$$N_t(\varepsilon) = \frac{N_{tot}}{\sqrt{\pi}kT_c} \exp\left[-\left(\frac{\varepsilon - \varepsilon_m}{kT_c}\right)^2\right] \tag{53}$$

and also a single discrete trap level:

$$N_t(\varepsilon) = N_{tot}\delta(\varepsilon - \varepsilon_m) \tag{54}$$

(where N_{tot} is the total trap density and T_c the characteristic temperature). The free-carrier generation rate was assumed to vary exponentially with the distance x from the front contact of the sample. Thus,

$$\Delta g(x) = \Delta g(0) \exp(-\alpha_0 x) \tag{55}$$

where α_0 is the light absorption coefficient.

In the figures below, the courses of the MPC phase shift, $\varphi_I(\omega)$, and amplitude, $\Delta I_m(\omega)$, computed using equations (28) and (29), are presented. In the cases of exponential and Gaussian trap distributions, the function $\tilde{\Phi}(\omega)$ was calculated numerically from the exact equation (A.3). The plots correspond to the idealized case of extremely small trap filling, due to the constant component of the exciting light—that is, to the limiting transition $\varepsilon_f \to \infty$. We intend to consider in detail the influence of trap saturation on the MPCs in a future paper. Each figure shows results for three different light absorption depths, determined by the values of $\alpha_0 d$. Solid lines indicate the curves corresponding to surface carrier generation; the dotted and dashed ones mark the curves for intermediate and low values of the light absorption coefficient, respectively. Additionally, the courses of the functions $\varphi(\omega)$, $\gamma(\omega)$, as well as of Re $\Delta n(x)$ for the case of surface carrier generation, are presented in separate figures.

Figure 1 presents the frequency dependencies of the phase angle $\varphi(\omega)$ (a) and 'damping coefficient' $\gamma(\omega)$ (b) of the free-carrier-density wave, calculated for the exponential trap distribution (52). For comparison, the curves computed from exact equations (30) and (31) (solid lines) as well as from the approximate ones (33) and (34) (dashed lines) are given. The figure shows that both the exact and approximate functions $\varphi(\omega)$ and $\gamma(\omega)$ increase with frequency as ω^α (where $\alpha = T/T_c$ is the dispersion parameter). However, there exist meaningful differences between the values of the corresponding multiplicative coefficients, particularly for the function $\varphi(\omega)$. The additional calculations show that the above-mentioned discrepancies gradually diminish with decreasing value of α. It should be recalled that analogous approximations are used in the theory of MPCs, measured in coplanar-electrode configurations (see, e.g., [2, 3]).

Figure 2 displays the phase shift (a) and the amplitude (b) of the MPC versus modulation frequency, calculated for the exponential trap distribution. All of the features of the MPCs discussed in the previous section can be recognized from the plots. As can be seen, for limiting cases of low and high modulation frequencies both the phase shift and the amplitude of the MPC are almost independent of the light absorption coefficient, except for the multiplicative factors. In the initial frequency domain the phase shift increases as ω^α, whereas in the high-frequency region the amplitude decays like $\omega^{-\alpha}$, in accordance with equations (44) and (38). In the intermediate-frequency domain the MPC phase shift shows oscillations being more and

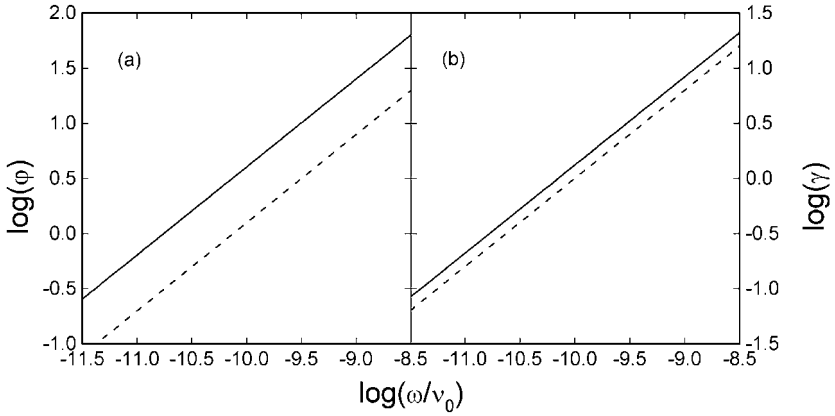

Figure 1. The phase angle (a) and 'damping coefficient' (b) of the free-carrier-density wave for exponential trap distribution. Solid lines correspond to exact equations (30) and (31); the dashed ones relate to approximate equations (33) and (34). The calculations were carried out for $T/T_c = 0.8$, $\tau_0\nu_0 = 10^{-5}$ and $C_t N_{tot}/\nu_0 = 10^{13}$.

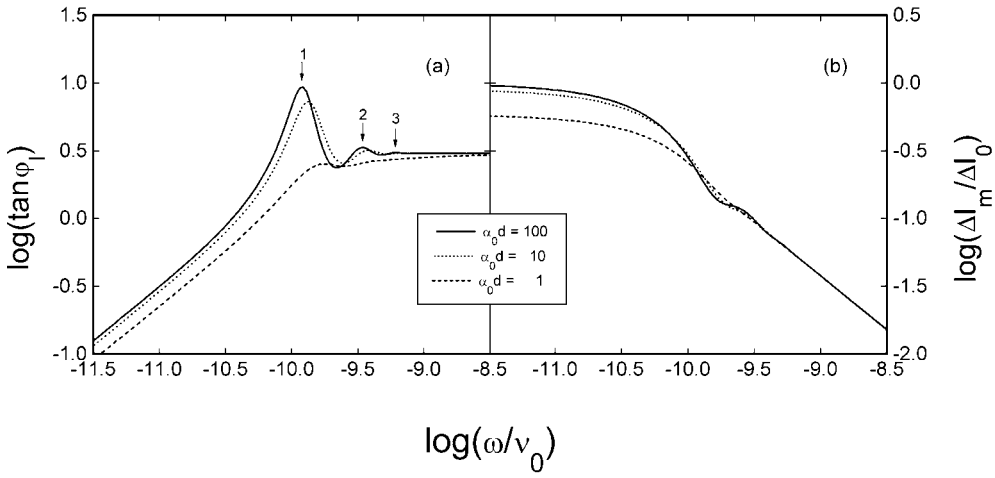

Figure 2. The MPC phase shift (a) and amplitude (b) for exponential trap distribution and three different light absorption depths. The arrows mark the positions of maxima of $\varphi_I(\omega)$, calculated from (50) and (51). The parameters are as for figure 1.

more strongly damped with the increase of ω, and the MPC amplitude exhibits some anomalous behaviour in the same frequency range. For increasing light absorption depth, the oscillations of $\varphi_I(\omega)$ gradually disappear and their maxima shift towards higher frequencies. The results given refer to relatively high values of the dispersion parameter $\alpha = 0.8$—that is, to the case of weakly dispersive transport. With decreasing α, the oscillations of $\varphi_I(\omega)$ become less and less distinct.

Figure 3 presents the spatial distributions of free carriers for the case of exponential distribution of traps and surface-absorbed light, computed from equation (27). The calculation parameters were the same as in figures 1 and 2. The normalization factor for the carrier density equals $\Delta n_0 = \Delta I_0 d/eS\mu_0 V$, where ΔI_0 is given by equation (37). The plots (a), (b) and (c) relate in turn to the values of ω corresponding to the maxima of the MPC phase shift

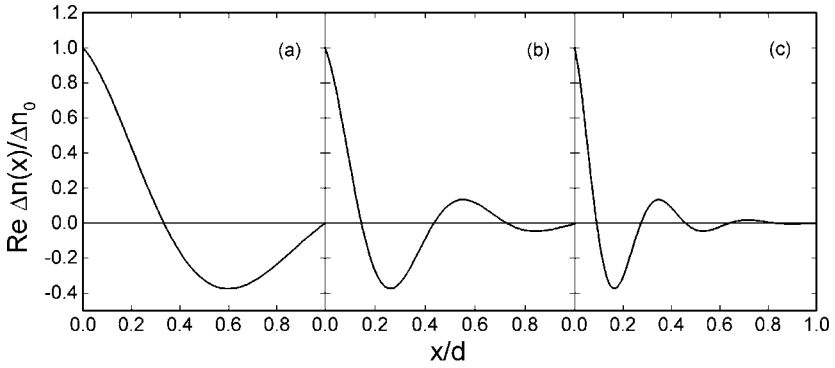

Figure 3. Spatial distributions of free carriers (real parts of oscillating terms), corresponding to figure 2 with $\alpha_0 d = 100$. The plots (a), (b) and (c) are obtained for frequencies corresponding to the maxima of $\varphi_I(\omega)$ in figure 2(a).

from figure 2(a). One can recognize that the phase angle φ of the oscillating carrier density $\Delta n(d)$ is equal, respectively, with a good accuracy, to $\varphi_1 = 3\pi/2$ (a), $\varphi_2 = 7\pi/2$ (b) and $\varphi_3 = 11\pi/2$ (c), in accordance with the formula (49). The figure illustrates also the stronger and stronger damping of the free-carrier-density wave with the increase of frequency.

Figure 4 shows the functions $\varphi(\omega)$ and $\gamma(\omega)$, calculated from the exact and approximate formulae for the Gaussian trap distribution (53). The calculation parameters are chosen in such a manner that the inequality $\varepsilon_0(\omega) > \varepsilon_m$ holds throughout the entire frequency range. In this case, the differences between the exact and approximate values become less significant with increasing frequency for both functions. The approximation of the function $\gamma(\omega)$ is again better than that of the function $\varphi(\omega)$.

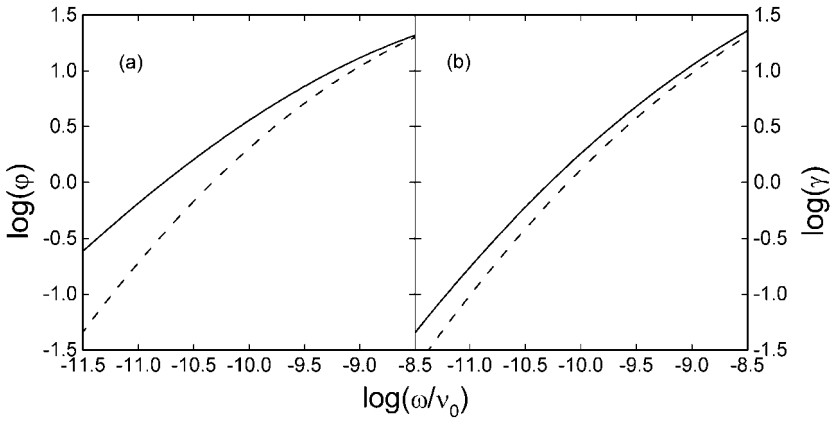

Figure 4. The phase angle (a) and 'damping coefficient' (b) of the free-carrier-density wave for Gaussian trap distribution. Solid and dashed lines denote respectively exact and approximate results. The parameters are: $\varepsilon_m/kT = 16$, $T/T_c = 0.25$, $\tau_0\nu_0 = 2\times10^{-11}$ and $C_t N_{tot}/\nu_0 = 10^{13}$.

Figure 5 shows the phase shift (a) and the amplitude (b) of the MPC, obtained for a Gaussian trap distribution. The carrier transport is here more dispersive than in the case corresponding to figure 2. For this reason, the oscillations of the phase shift of the MPC almost disappear. One can distinguish only a single wide maximum of $\varphi_I(\omega)$.

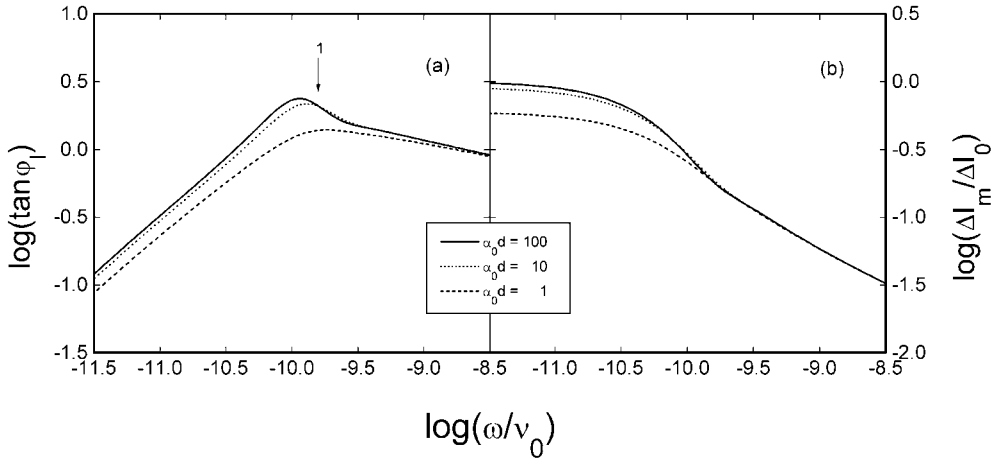

Figure 5. The MPC phase shift (a) and amplitude (b) for Gaussian trap distribution and different values of the light absorption coefficient. The arrow indicates the position of the calculated maximum of $\varphi_I(\omega)$. The parameters are as for figure 4.

Figure 6 presents the frequency dependence of the MPC phase shift and amplitude for the case of a single discrete trap level (54). The asymptotic behaviour of the phase shift is given by the formulae $\varphi_I(\omega) \propto \omega$ for $\omega \ll \omega_e, 1/\tau_r(\varepsilon_m)$ and $\varphi_I(\omega) \propto \omega^{-1}$ for $\omega \gg \omega_e, 1/\tau_r(\varepsilon_m)$, according to (30), (31), (39) and (44). In the intermediate range of frequencies the course of the curves is similar to that from figure 2, with the exception of clearly visible oscillations of $\Delta I_m(\omega)$. One has to stress that the value of the MPC phase shift exceeds $\pi/2$ in a certain frequency interval and thus the proper root of the equation

$$\tan\varphi_I = -\mathrm{Im}\,\Delta I/\mathrm{Re}\,\Delta I$$

must be chosen (cf. equations (28) and (29)). We have assumed that the function $\varphi_I(\omega)$ is a continuous one and that $\lim_{\omega\to 0}\varphi_I(\omega) = 0$.

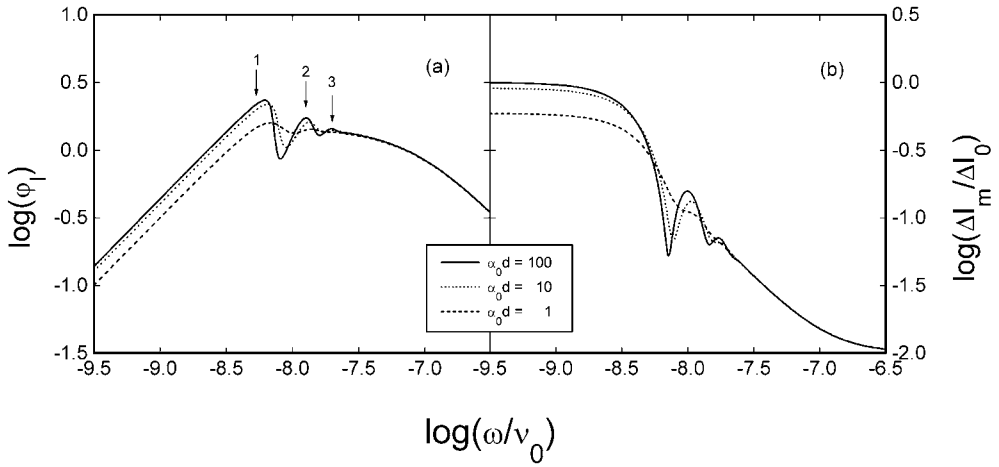

Figure 6. The MPC phase shift (a) and amplitude (b) for a discrete trap level and several light absorption depths. The arrows indicate the computed frequencies, corresponding to the maxima of $\varphi_I(\omega)$. The values of the parameters are: $\varepsilon_m/kT = 16$, $\tau_0\nu_0 = 10^{-11}$ and $C_t N_{tot}/\nu_0 = 10^{13}$.

Figure 7 shows the spatial distributions of free carriers for the case of a discrete trap level in an analogous manner to figure 3. One can notice that the individual values of the phase angle φ do not fulfil exactly equation (49), particularly in plot (a). This is because the functions $\varphi(\omega)$ and $\gamma(\omega)$ strongly vary in the corresponding frequency region. One also observes the damping of the free-carrier wave, which is more significant for higher frequencies.

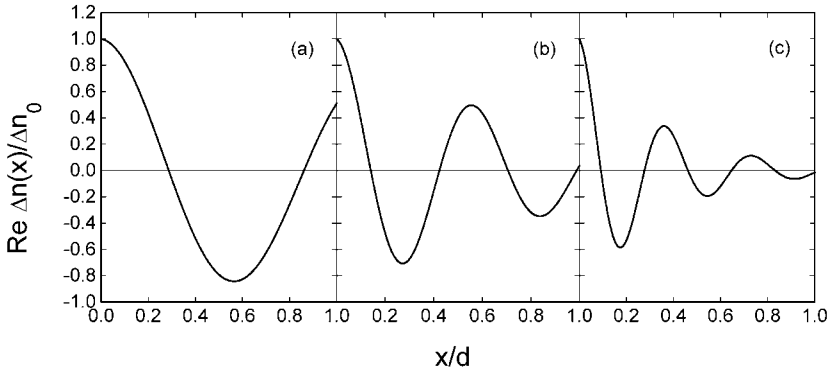

Figure 7. Spatial distributions of free carriers for a discrete trap level, corresponding to figure 6 with $\alpha_0 d = 100$. The plots (a), (b) and (c) are obtained for frequencies corresponding to the maxima of $\varphi_I(\omega)$ in figure 6(a).

5. Conclusions

On the basis of the results obtained, the following conclusions can be drawn. The forms of the MPC phase shift and amplitude in the low- and high-frequency domains are almost independent of the light absorption coefficient. In these frequency ranges, both the phase shift and the amplitude of the photocurrent can be described using the derived approximate formulae, and the energetic DOS can be calculated making use of the methods known from previous papers. In the intermediate-frequency range, for weakly dispersive carrier transport and surface light absorption, the MPC phase shift exhibits damped oscillations. The oscillations gradually disappear with increasing light absorption depth. The essential point is that the presence of the phase-shift oscillations enables us also to determine the form of the DOS. This can be done on the basis of formulae (50) and (51) for experimental data corresponding to different applied voltages and/or to different sample thicknesses. It is worth stressing that all the results obtained here and in the earlier papers on the subject [7, 11, 15] apply solely in the frequency range $\omega \gg 1/\tau_M$ (cf. section 3.1). The given condition may not be fulfilled in the case of MPC measurements on highly photoconductive samples.

Appendix A. Quasi-Fermi-level approximation

From equation (2) we obtain the following formula relating the dc components of trapped- and free-carrier densities:

$$n'_{t0}(x, \varepsilon) = \frac{N_t(\varepsilon)}{1 + 1/C_t n_0(x)\tau_r(\varepsilon)}. \tag{A.1}$$

Therefore, the energetic density of empty traps

$$N_t(\varepsilon) - n'_{t0}(x, \varepsilon) = \frac{N_t(\varepsilon)}{1 + C_t n_0(x)\tau_r(\varepsilon)} \tag{A.2}$$

and formula (19) for $\tilde{\Phi}(x)$ can be rewritten as

$$\tilde{\Phi}(x) = C_t \int_0^\infty \frac{N_t(\varepsilon)\,\mathrm{d}\varepsilon}{[1 + C_t n_0(x)\tau_r(\varepsilon)]\,[\mathrm{i}\omega + C_t n_0(x) + 1/\tau_r(\varepsilon)]}. \tag{A.3}$$

It is seen that the trapped-carrier distribution and, in consequence, the form of the function $\tilde{\Phi}(x)$ are characterized mainly by the position of the quasi-Fermi level, $\varepsilon_f(x)$, given implicitly by

$$\tau_r\left[\varepsilon_f(x)\right] = 1/C_t n_0(x). \tag{A.4}$$

In the case of a slowly varying trap density, the trapped-carrier distribution is approximately described by

$$n'_{t0}(x, \varepsilon) \simeq N_t(\varepsilon) H\left[\varepsilon - \varepsilon_f(x)\right]$$

where $H[\cdots]$ is the unit step function. If the demarcation energy $\varepsilon_0 < \varepsilon_f(x)$ (cf. (35)), the dominant contribution to the integral (A.3) originates from the interval $0 \leqslant \varepsilon \leqslant \varepsilon_f(x)$, where the terms involving $C_t n_0(x)$ may be omitted. In this way, from (A.3) and (A.4) one obtains equations (22) and (23) given in the text.

Appendix B. Solution of the linearized transport equations

Making use of Poisson's equation (13) and integrating equation (11) over x subject to the conditions (14) and (15), we get the formula

$$\mu_0\left[E_0(x)\,\Delta n(x) + n_0(x)\,\Delta E(x)\right] + \frac{\mathrm{i}\omega\kappa\kappa_0}{e}\left[\Delta E(x) - \Delta E(0)\right] = \int_0^x \Delta g(x')\,\mathrm{d}x'. \tag{B.1}$$

From equations (13) and (18) there follows the relationship

$$\Delta n(x) = \frac{\kappa\kappa_0}{e[1 + \tilde{\Phi}(x)]}\frac{\mathrm{d}\,\Delta E(x)}{\mathrm{d}x}. \tag{B.2}$$

Inserting (B.2) into (B.1) one obtains the differential equation for $\Delta E(x)$:

$$\frac{\mu_0 E_0(x)}{1 + \tilde{\Phi}(x)}\frac{\mathrm{d}\,\Delta E(x)}{\mathrm{d}x} + \left[\mathrm{i}\omega + \frac{1}{\tau_M(x)}\right]\Delta E(x) = \frac{e}{\kappa\kappa_0}\,\Delta g(x) + \mathrm{i}\omega\,\Delta E(0) \tag{B.3}$$

where

$$\tau_M(x) = \frac{\kappa\kappa_0}{e\mu_0 n_0(x)} \tag{B.4}$$

is the Maxwell relaxation time referring to the carrier density $n_0(x)$. The solution of equation (B.3) has an involved form but simplifies considerably when the term $\Delta E(x)/\tau_M(x)$ can be neglected. The corresponding criterion is

$$\omega\tau_M(x) \gg \frac{|\mathrm{Im}\,\tilde{\Phi}(x)|}{1 + \mathrm{Re}\,\tilde{\Phi}(x)}, \frac{1 + \mathrm{Re}\,\tilde{\Phi}(x)}{|\mathrm{Im}\,\tilde{\Phi}(x)|} \qquad 0 \leqslant x \leqslant d. \tag{B.5}$$

Usually $\mathrm{Re}\,\tilde{\Phi} \gg 1$, as noted in section 3.1. Moreover, in the case of dispersive transport, $\mathrm{Re}\,\tilde{\Phi}$ and $\mathrm{Im}\,\tilde{\Phi}$ are of the same order. Then, from (B.5) there results the condition $\omega \gg 1/\tau_M(x)$, $0 \leqslant x \leqslant d$.

In the approximation considered, the solution of equation (B.3) has the form

$$\Delta E(x) = \frac{e}{\mathrm{i}\omega\kappa\kappa_0}\int_0^x \Delta g(x')\left\{1 - \exp\left[-\frac{\mathrm{i}\omega}{\mu_0}\int_{x'}^x \frac{1 + \tilde{\Phi}(x'')}{E_0(x'')}\,\mathrm{d}x''\right]\right\}\mathrm{d}x' + \Delta E(0). \tag{B.6}$$

Making use of equation (B.2), one then obtains expression (25) for $\Delta n(x)$. In order to calculate the MPC it is convenient to rewrite the formula (24), using equation (B.1), as

$$\Delta I = \frac{eS}{d}\int_0^d \left\{\int_0^x \Delta g(x')\,\mathrm{d}x' - \frac{\mathrm{i}\omega\kappa\kappa_0}{e}\left[\Delta E(x) - \Delta E(0)\right]\right\}\mathrm{d}x. \tag{B.7}$$

Then, inserting expression (B.6), one gets the formula (26).

References

[1] Oheda H 1981 *J. Appl. Phys.* **62** 6693
[2] Brüggemann R, Main C, Berkin J and Reynolds R 1990 *Phil. Mag.* B **62** 29
[3] Hattori K, Niwano Y, Okamoto H and Hamakawa Y 1991 *J. Non-Cryst. Solids* **137+138** 363
[4] Aktas G and Skarlatos Y 1984 *J. Appl. Phys.* **55** 3577
[5] Schumm G, Nitsch K and Bauer G H 1988 *Phil. Mag.* B **58** 411
[6] Kounavis P and Mytilineou E 1993 *J. Non-Cryst. Solids* **164-166** 623
[7] Hattori K, Adachi Y, Anzai M, Okamoto H and Hamakawa Y 1994 *J. Appl. Phys.* **76** 2841
[8] Kounavis P and Mytilineou E 1999 *J. Phys.: Condens. Matter* **11** 9105
[9] Longeaud C and Kleider J P 1992 *Phys. Rev.* B **45** 11 672
[10] Longeaud C and Kleider J P 1993 *Phys. Rev.* B **48** 8715
[11] Schumm G and Bauer G H 1989 *Phys. Rev.* B **39** 5311
[12] Brüggemann R, Schumm G, Main C, Berkin J and Bauer G H 1991 *J. Non-Cryst. Solids* **137+138** 359
[13] Amato G, Giorgis F, Fizzotti F and Manfredotti C 1993 *Solid State Commun.* **86** 277
[14] Cohen J D and Zhong F 1995 *J. Non-Cryst. Solids* **190** 123
[15] Tomaszewicz W 1990 *Phil. Mag. Lett.* **61** 237
[16] Blakney R M and Grunwald H P 1967 *Phys. Rev.* **159** 659
[17] Grygiel P and Tomaszewicz W 1997 *J. Phys.: Condens. Matter* **9** 10 381
[18] Lampert M A and Mark P 1970 *Current Injection in Solids* (New York: Academic)
[19] Seynhaeve G, Adriaenssens G J, Michiel H and Overhof H 1988 *Phil. Mag.* B **58** 421